Article

Excitonic resonances control the temporal dynamics of nonlinear optical wave mixing in monolayer semiconductors

Jonas M. Bauer[1,5], Lijue Chen [1,2,5], Philipp Wilhelm[1], Kenji Watanabe [3], Takashi Taniguchi [4], Sebastian Bange [1], John M. Lupton [1] and Kai-Qiang Lin [1]✉

Monolayer semiconductors are an emerging platform for strong nonlinear light–matter interactions that are enhanced by the giant oscillator strength of tightly bound excitons. Little attention has been paid to the impact of excitonic resonances on the temporal dynamics of such nonlinearities, since harmonic generation and optical wave mixing are generally considered instantaneous processes. We find that a significant time difference, ranging from −40 to +120 fs, is necessary between two light pulses for optimal sum-frequency generation (SFG) and four-wave mixing (FWM) to occur from monolayer WSe_2 when one of the pulses is in resonance with an excitonic transition. These resonances involve both band-edge A excitons and high-lying excitons that comprise electrons from conduction bands far above the bandgap. Numerical simulations in the density-matrix formalism rationalize the distinct dynamics of SFG and FWM. The interpulse delays for maximal SFG and FWM are governed primarily by the lifetime of the one-photon and two-photon resonant states, respectively. The method therefore offers an unconventional probe of the dynamics of excitonic states accessible with either one-photon or two-photon transitions. Remarkably, the longest delay times occur at the lowest excitation powers, indicating a strong nonlinearity that offers exploration potential for excitonic quantum nonlinear optics.

Nonlinear optical wave-mixing processes[1,2] such as second-harmonic generation (SHG), SFG and FWM are important in the design of lasers[3], the characterization of ultrashort laser pulses, in photon detection and in optical sensing[4]. Since light does not interact appreciably with itself, the source of an optical nonlinearity is the electronic polarization of a material that is driven by several incident light fields[1]. Conventional descriptions of nonlinear polarization emphasize the perspective that the polarization measured is the product of several incident electric fields with the nonlinear susceptibility at a set of exact frequencies. Such descriptions are only strictly applicable under continuous-wave conditions[2]. Wave mixing is thus generally described as a quasi-instantaneous parametric process, for which the quantum state of matter does not change. Ultimately, this assumption can only be true for the initial and final states of the interaction since, in the

[1]Department of Physics, University of Regensburg, Regensburg, Germany. [2]College of Chemistry and Chemical Engineering, Xiamen University, Xiamen, China. [3]Research Center for Functional Materials, National Institute for Materials Science, Tsukuba, Japan. [4]International Center for Materials Nanoarchitectonics, National Institute for Materials Science, Tsukuba, Japan. [5]These authors contributed equally: Jonas M. Bauer, Lijue Chen. ✉e-mail: kaiqiang.lin@ur.de
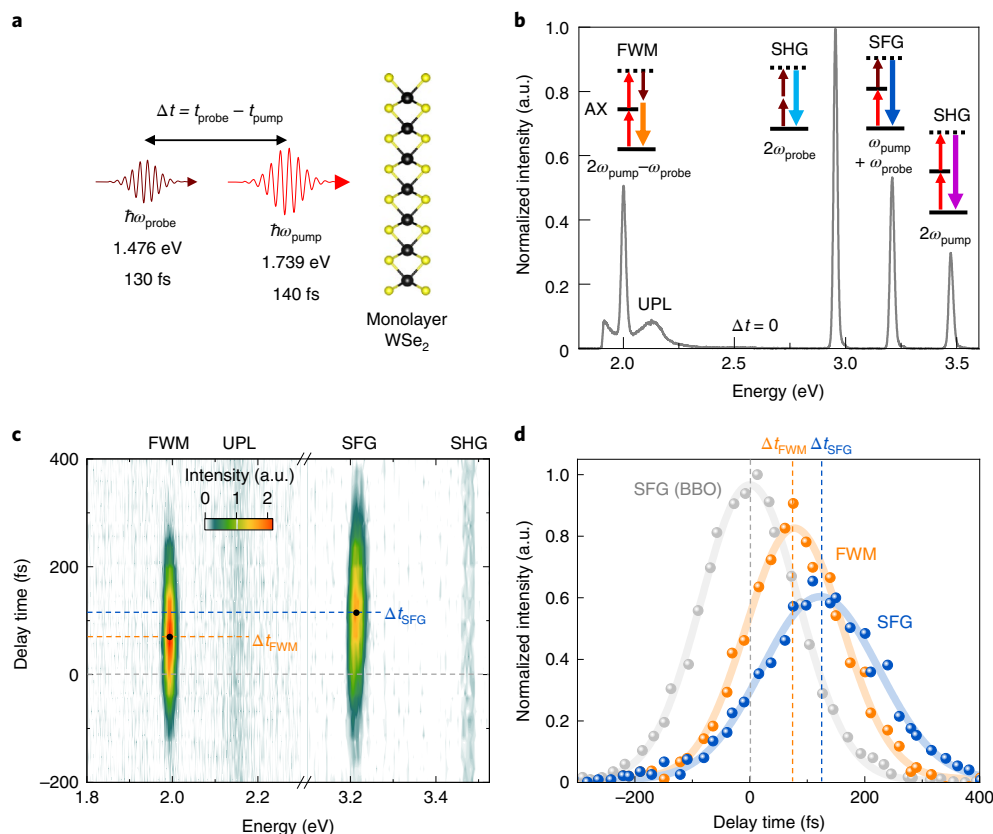
Fig. 1 | Delayed SFG and FWM from monolayer WSe₂. a, Schematic illustration of the nonlinear optical wave-mixing experiment with two laser pulses at 1.739 eV and 1.476 eV focused onto a monolayer WSe₂ at a temperature of 5 K. **b**, Spectrum of the light generated, detected in reflection geometry. FWM, UPL, SHG and SFG appear for a time delay $\Delta t = 0$ between the position of the peak intensities of the pump and probe laser impulses as defined in **a**. The pump beam is in resonance with the AX. **c**, Two-colour optical wave-mixing spectrum as a function of Δt. Maximal SFG and FWM intensities appear at non-zero delay times. **d**, Spectrally integrated intensity of SFG (blue) and FWM (orange) as a function of Δt. The SFG intensity of a 100-μm-thick BBO crystal (grey) in place of the WSe₂ sample is shown as a function of Δt to provide a zero-time-delay reference.

quantum picture of light–matter interactions, every interaction process inevitably changes the quantum state for both photons and electrons. In the density-matrix representation of the electronic quantum states, the expectation value for the observable polarization $P(t) = \langle \hat{\mu}\hat{\rho}(t)\rangle$ (where $\hat{\mu}$ is the dipole-moment matrix and $\hat{\rho}$ is the density matrix) therefore generally contains an integration over all possible quantum pathways, involving all transitions with non-zero dipole-moment matrix elements μ_{ij} for all possible times and frequencies at which electric fields are present[1,5]. This approach has proved powerful for multidimensional coherent spectroscopy[6], where a nonlinear response is excited by multiple laser pulses. An important consequence of this extended picture of wave mixing is that parametric interactions progress via diagonal elements ρ_{ii} of the density matrix, which means that they can be sensitive not only to dephasing of transition dipoles but also to excited-state lifetimes as well as to state depletion and transition saturation.

Transition metal dichalcogenide (TMDC) monolayers have emerged as an intriguing two-dimensional medium to accommodate strong light–matter interactions[7–11]. As direct-gap semiconductors with weak dielectric screening, TMDC monolayers host strongly bound excitons near the K-points of the Brillouin zone[12–14]. Owing to broken inversion symmetry, the materials exhibit nonlinear responses of both even and odd order, suggesting a wide range of application potential in nonlinear wave mixing[7,11,15,16]. Among other effects, the giant excitonic enhancement in nonlinearity[7,15,17] near resonance exhibited by these materials has enabled SHG and SFG under continuous-wave irradiation[18,19]. A pronounced splitting of the SHG spectrum due to Rabi

flopping of the excited-state population occurs even under comparatively weak pulsed-laser excitation[20], and is associated with light-driven quantum interference between the excitation pathways of the bound band-edge A exciton (AX) and a two-photon resonant high-lying exciton (HX) involving upper conduction bands at the same ±K-points[19]. As shown via experiment and *GW* plus Bethe–Salpeter equation (*GW*–BSE) theory, the energy of the HX species happens to be close to twice that of the AX, forming an almost evenly spaced three-level system[19]. Such a ladder-type excitonic structure offers a new all-solid-state platform for coherent nonlinear optical processes such as electromagnetically induced transparency[21]. This three-level system is intrinsic to the unusual band structure of the monolayer[19] and differs fundamentally from conventional biexcitonic systems[22], where a high density of excitons is needed for two excitons to meet in space to form a bound state that contributes to the nonlinear interaction[23,24]. Besides SHG and SFG, single-pass optical parametric amplification has also been demonstrated in TMDC monolayers[25]. Although excitonic enhancement of the nonlinear light–matter interaction appears to be well established, it is not at all clear whether and how excitonic transitions affect the temporal dynamics of nonlinear interactions.

Figure 1a illustrates the setup for a two-colour excitation experiment using ultrafast laser pulses of 130–140 fs length and 80 MHz repetition rate at 713 nm (with an energy $\hbar\omega_{\text{pump}} = 1.739$ eV) and 840 nm ($\hbar\omega_{\text{probe}} = 1.476$ eV), impinging on an exfoliated WSe₂ monolayer with a time difference $\Delta t = t_{\text{probe}} - t_{\text{pump}}$. For notational convenience, we refer to the pulse resonant with the excitonic transition as the 'pump' pulse and the pulse detuned far from any excitonic resonance as the
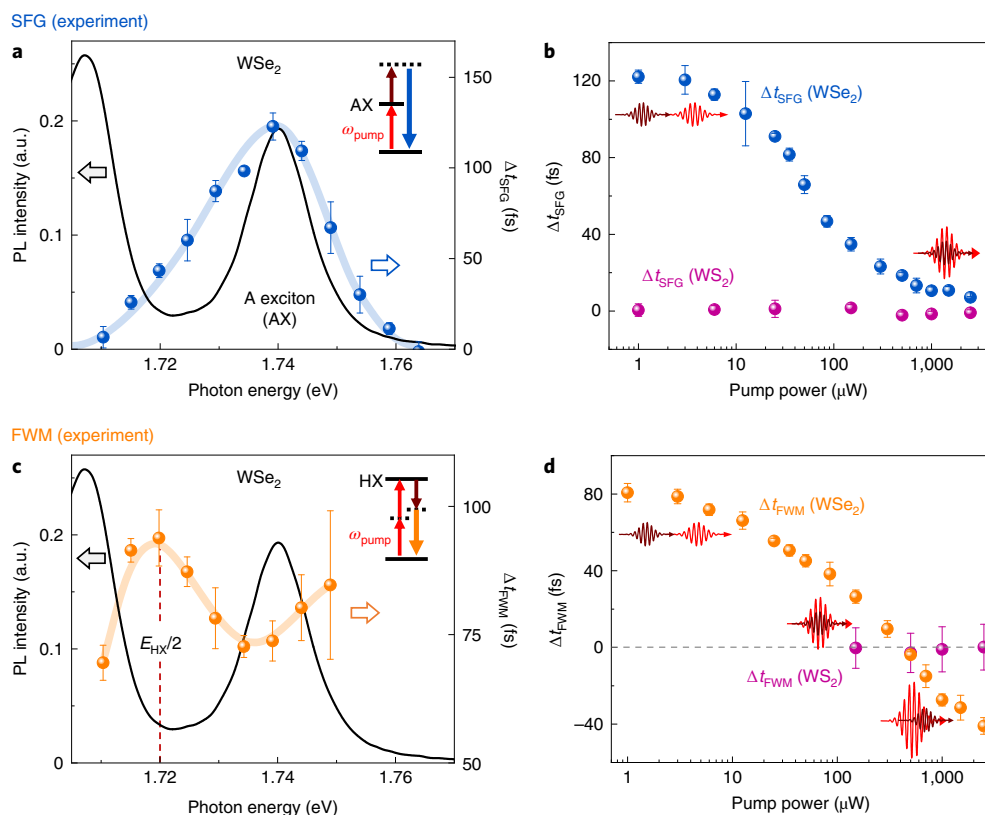
Fig. 2 | Excitonic effects on the delay time for maximal SFG and FWM. a,
Comparison of the PL spectrum of monolayer WSe_2 (black curve) with the delay
time for maximal SFG, Δt_{SFG}, as a function of the pump photon energy (blue
spheres). The power of the probe beam is set to 400 µW (176 µJ cm^{-2}) at 1.476 eV
and the pump beam is set to 3 µW (1.32 µJ cm^{-2}). The blue line is a guide for
the eye. **b,** Dependence of Δt_{SFG} on the pump beam power for monolayer WSe_2
(blue spheres) and monolayer WS_2 (purple spheres) using $\hbar\omega_{pump} = 1.739$ eV in
resonance with the AX, $\hbar\omega_{probe} = 1.476$ eV and a probe-beam power of 400 µW. **c,**
PL spectrum of monolayer WSe_2 (black curve) compared with the delay time for
maximal FWM, Δt_{FWM}, as a function of the pump photon energy (orange spheres).

The measurement conditions are the same as in **a**. The orange line is a guide for
the eye. The dashed line marks the two-photon resonance with an HX, which is
congruent with the position of the dip in the SHG spectrum (see Supplementary
Fig. 4). **d,** Dependence of Δt_{FWM} on the pump power for monolayer WSe_2
(orange spheres) and monolayer WS_2 (purple spheres) using $\hbar\omega_{pump} = 1.739$ eV,
$\hbar\omega_{probe} = 1.476$ eV and a probe-beam power of 400 µW. The red and dark-red
wave packets indicate the temporal relation of the pump and probe pulses. The
grey dashed line marks the zero time delay. Throughout, the error bars are the
standard deviation of the results of three independent measurements on the
same sample position.

'probe' pulse, although we do not limit Δt to positive values nor do we
restrict the probe beam to lower intensities than the pump beam. The
sample is cooled to a temperature of 5 K using a microscope cryostat
and excited through a long-working-distance microscope objective
with a numerical aperture (NA) of 0.6. Details of the setup are shown
in Supplementary Fig. 1. Figure 1b plots a representative spectrum
of the upconverted radiation detected in back-reflected geometry
through the same objective, for a time delay of $\Delta t = 0$ and using a
680 nm (1.82 eV) short-pass filter. Five characteristic spectral contri-
butions are identified by their frequencies: SHG of the pump beam
at $2\omega_{pump}$, SFG of the pump and probe beams at $\omega_{pump} + \omega_{probe}$, SHG of
the probe beam at $2\omega_{probe}$, FWM at $2\omega_{pump} - \omega_{probe}$ and upconverted
photoluminescence (UPL) of the so-called 'B exciton' close to the
FWM peak[19]. As monolayer TMDCs have giant second- and third-order
optical susceptibilities[7], both second-order nonlinear processes, such
as SFG, and third-order nonlinear processes, such as FWM, are very
efficient[15,25,26]. Monolayer TMDCs therefore constitute broadband opti-
cal frequency mixers[27]. Excitation and detection through the high-NA
objective bypasses most of the constraints on beam direction due to
the conservation of momentum that is usually necessary for efficient
nonlinear wave mixing[2].

Figure 1c shows a two-dimensional map of the upconverted radia-
tion as a function of the pump–probe delay time Δt. As expected, nei-
ther the SHG of either the pump or probe beam nor the UPL show any

dependence on the coincidence of pump and probe impulses. On the
other hand, both SFG and FWM are sensitive to Δt. However, the maxi-
mum efficiency of these two processes does not occur at zero delay,
which is surprising given that parametric, instantaneous nonlinear
optical wave mixing should be most effective for an optimal temporal
pulse overlap. As the time delay between the two laser impulses is sensi-
tive to group delays accumulated in the optical setup, the zero delay is
referenced to the SFG response of a 100-µm-thick beta-barium borate
(BBO) crystal cut at 29.2°, which is placed next to the monolayer WSe_2
sample as detailed in Supplementary Fig. 1. Figure 1d shows the SFG
intensity from the BBO crystal (grey spheres) as well as the spectrally
integrated SFG (blue spheres) and FWM (orange spheres) intensities
of the WSe_2 sample as a function of the delay time, along with Gaussian
fits (lines). The dashed lines mark the centre of each Gaussian, with
the FWM peaking at the delay time $\Delta t_{FWM} = 80$ fs (orange) and the SFG
peaking at $\Delta t_{SFG} = 120$ fs (blue).

To examine the role of excitons in the retardation of these non-
linear processes, we perform the measurements as a function of the
photon energy. Figure 2a shows the dependence of the time delay
for maximal SFG (blue spheres) on the energy of the pump laser for a
fixed probe energy $\hbar\omega_{probe} = 1.476$ eV. Comparison with the photolumi-
nescence (PL) spectrum (black curve) reveals that the largest Δt_{SFG} of
120 fs is reached precisely when the pump laser is in resonance with the
AX. Under off-resonance detuning, Δt_{SFG} decreases to zero. Since both
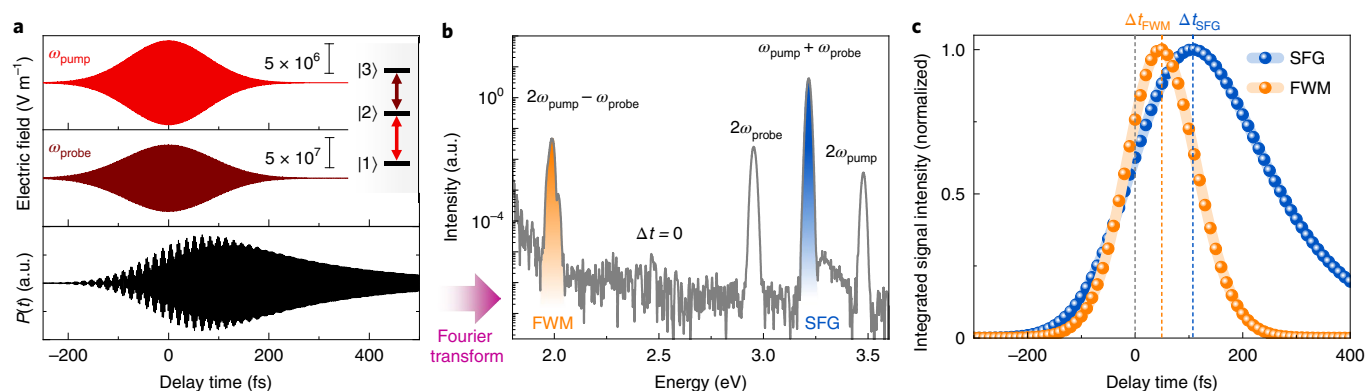
Fig. 3 | Nonlinear optical wave-mixing spectroscopy simulated using the density-matrix formalism. a, Illustration of electric fields and electronic polarization in the numerical simulation model used to describe the population evolution in a ladder-type three-level excitonic system. **b**, Representative calculated optical wave-mixing spectrum at a delay time of zero. The FWM contribution is highlighted in orange and SFG is marked blue. The noise floor corresponds to the numerical precision used for the simulation. **c**, Spectrally integrated intensity of SFG and FWM signals as a function of the delay time between the pump and probe pulses. Δt_{SFG} and Δt_{FWM} mark the delay times for the maximal intensities of SFG and FWM, respectively. The grey dashed line marks the zero time delay. The pump at 1.739 eV is set to a power of 1 μW (0.44 μJ cm^{-2}) and the probe at 1.476 eV is set to 200 μW (88 μJ cm^{-2}).

the pump and probe pulses are short and therefore spectrally broad, the peak in the energy dependence of Δt_{SFG} appears to be broader than the PL peak of the AX.

If the delay is caused by an excitonic resonance, it should depend on the excitation density. Figure 2b shows Δt_{SFG} for monolayer WSe$_2$ (blue spheres) as a function of the pump power for $\hbar\omega_{pump}$ = 1.739 eV, $\hbar\omega_{probe}$ = 1.476 eV and a probe-beam power of 400 μW (0.18 mJ cm^{-2}). On increasing the pump power by three orders of magnitude (below the Mott transition, see Supplementary Note 2), Δt_{SFG} decreases from >120 fs to close to zero. Experimentally, this can lead to the counterintuitive phenomenon of an increasing SFG intensity with a decreasing pump power, as shown in Supplementary Fig. 2. It may be tempting to assign such a decrease in Δt_{SFG} to the decrease of the AX lifetime with increasing excitation density, as observed in transient intra- and interband spectroscopy[28] and optical two-dimensional Fourier-transform spectroscopy[29]. However, as we demonstrate below, this decrease can also be rationalized in terms of the dynamics of Rabi flopping[30]. In contrast to the effect of varying the pump power, Supplementary Fig. 3a shows that comparable changes in the probe power do not affect the Δt_{SFG}. To eliminate the possibility of optical artefacts and establish a further reference for the measurements, the experiments were repeated for monolayer WS$_2$ in place of the WSe$_2$ sample. Since the bandgap of monolayer WS$_2$ is approximately 0.3 eV larger than that of monolayer WSe$_2$, the lasers will not be in resonance with excitonic transitions. Indeed, Δt_{SFG} from monolayer WS$_2$ (purple spheres in Fig. 2b) is close to zero over the entire range of pump power.

The amplitudes of the FWM signals detected simultaneously are shown in Fig. 2c,d (orange spheres). In contrast to Δt_{SFG}, the delay time for maximum FWM, Δt_{FWM}, does not peak at the pump photon energy of the AX resonance (Fig. 2c), but rather at an energy that also gives rise to quantum interference in the SHG as shown in Supplementary Fig. 4 (refs. [19,20]). This quantum interference arises due to the high-lying excitonic state HX, which lies at 3.44 eV and contributes to the delay Δt_{FWM} through a two-photon resonance with the pump laser, as illustrated in the inset of Fig. 2c. As found for Δt_{SFG}, Δt_{FWM} decreases with increasing pump power (orange circles in Fig. 2d) and is independent of the probe power (Supplementary Fig. 3b) and the probe photon energy (Supplementary Fig. 5c). Unexpectedly, however, Δt_{FWM} drops below zero in the high-pump-power regime: above 1 mW (0.44 mJ cm^{-2}), the centre of the probe pulse must reach the sample 40 fs before the centre of the pump pulse for maximum efficiency of FWM. As reported in Supplementary Fig. 5a, the maximum values of |Δt_{SFG}| and |Δt_{FWM}| become

even larger for WSe$_2$ monolayer samples with hexagonal boron nitride (hBN) encapsulation. This change may conceivably arise from a suppression of local sample inhomogeneities[31,32] and a modification of the radiative decay rate due to a cavity effect[33]. The fact that the maximal values of Δt_{SFG} and Δt_{FWM} appear at the lowest powers of both the pump and probe beams (Supplementary Fig. 5b) demonstrates that strong nonlinear interactions extend into the regime of the low excitation densities, opening up avenues for further exploration of quantum nonlinear optics[34,35].

While the change in the interpulse delay for SFG can, in principle, be rationalized through a pump-power dependence of a sufficiently long-lived excitonic resonance[29], the negative Δt_{FWM} is not straightforward to explain. To account for the excitonic resonances, instead of following the conventional analysis of the parametric light–matter interaction up to fixed nonlinear order[1,2], we use a full time-dependent solution of the density-matrix dynamics in the presence of the laser field (see Methods for details). This approach uses a simplified state description borrowed from atomic optics and has been successfully employed before to describe the effect of Rabi flopping in the unusual SHG spectra from monolayer WSe$_2$ (ref. [20]). For realistic excitation conditions, the laser fields are modelled as Gaussian pulses with parameters matching the experimental ones as illustrated in Fig. 3a. We describe the allowed eigenstates using a simple ladder-type three-level system shown in Fig. 3a, which consists of a ground state $|1\rangle$, the AX state $|2\rangle$ and the HX state $|3\rangle$. The detailed parameters used for the simulation, listed in the Supplementary Fig. 6 and Supplementary Table 1, are based on experimental conditions.

Figure 3b shows a calculated optical wave-mixing spectrum for the same spectral range as probed experimentally (Fig. 1b), at zero time delay between the pump and probe pulses ($\hbar\omega_{pump}$ = 1.739 eV and $\hbar\omega_{probe}$ = 1.476 eV). Five prominent peaks are identified, including FWM ($2\omega_{pump} - \omega_{probe}$), SHG ($2\omega_{pump}$ and $2\omega_{probe}$), and SFG ($\omega_{pump} + \omega_{probe}$). A six-wave-mixing feature ($3\omega_{pump} - 2\omega_{probe}$) appears at a higher pump fluence (see Supplementary Fig. 8). Figure 3c shows the result of calculating the spectrally integrated SFG and FWM intensities as a function of the delay time between the pump and probe pulses. Here, the pump laser is set to be resonant with state $|2\rangle$, with a low power of 1 μW (0.44 μJ cm^{-2}). The simulated maximal SFG intensity appears for a positive delay time of approximately 105 fs, which is close to the experimental value of 120 fs in Fig. 1d. The maximal FWM intensity appears at a delay time of 50 fs, which is somewhat smaller than the experimental result although it confirms the experimental trend that Δt_{FWM} tends to be smaller than Δt_{SFG}.
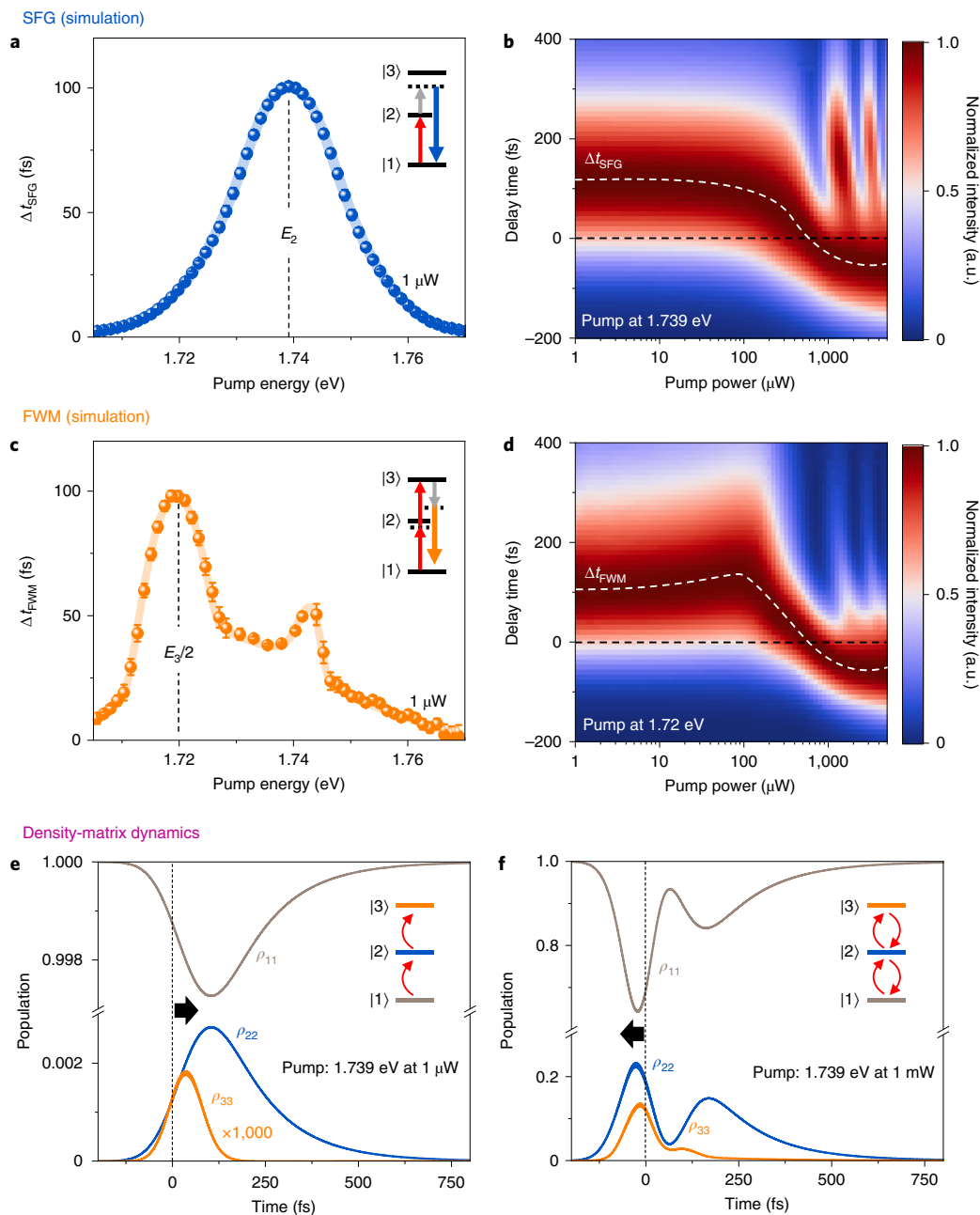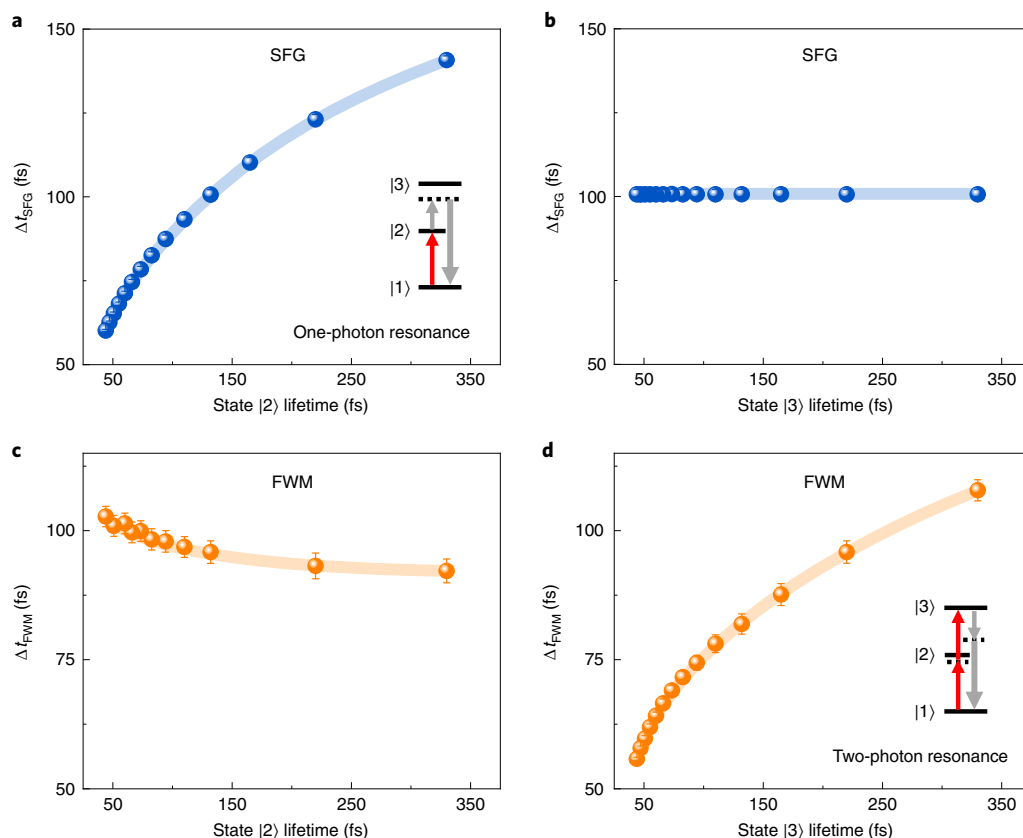
Fig. 4 | Simulated delay times for maximal SFG and FWM intensities. a, Delay time Δt_{SFG} for the maximal simulated SFG intensity as a function of the pump photon energy. The pump at 1.739 eV is set to a power of 1 μW (0.44 μJ cm^{-2}) while the probe at 1.476 eV is set to 200 μW (88 μJ cm^{-2}). **b**, Corresponding dependence of the intensity of SFG on the delay time as a function of pump power, with the pump in resonance with the $|1\rangle \rightarrow |2\rangle$ excitonic transition (AX) at 1.739 eV. **c**, Delay time for the maximal simulated FWM intensity, Δt_{FWM}, as a function of the pump photon energy. The pump power and the parameters for the probe beam are as in **a**. The error bars mark the uncertainty in peak position from fitting the numerical

results. The dashed line marks the energy for two-photon excitation of the HX (state $|3\rangle$). **d**, Corresponding dependence of the simulated FWM intensity on the delay time as a function of pump power, with the pump in two-photon resonance with the $|1\rangle \rightarrow |3\rangle$ (HX) transition. **e**, Density-matrix dynamics of the excitonic three-level system for a pump power of 1 μW, without the probe beam. State $|2\rangle$ reaches maximum occupancy at a delay time of 105 fs with respect to the centre of the pump pulse. **f**, Density-matrix dynamics for a pump power of 1 mW. State $|3\rangle$ reaches maximum occupancy before the arrival of the peak of the pump pulse, and all three states show pronounced Rabi oscillations.

Next, we investigate the influence of the pump power and photon energy on Δt_{SFG} and Δt_{FWM}. Figure 4a,c shows the dependence on the pump photon energy of Δt_{SFG} and Δt_{FWM} at a low pump power of 1 μW. The maximum SFG arises for a pump beam resonant with the $|1\rangle \rightarrow |2\rangle$ transition (the AX), whereas the maximum FWM is found when the pump laser is two-photon resonant with the $|1\rangle \rightarrow |3\rangle$ transition, that is, the HX. These resonant enhancements coincide with the experimental observations (Fig. 2a,c). Figure 4b,d plots the simulated pump-power

dependence of Δt_{SFG} and Δt_{FWM}. Both Δt_{SFG} and Δt_{FWM} drop with increasing power, qualitatively matching with experiments. The simulation, however, shows that both Δt_{SFG} and Δt_{FWM} become negative at high pump powers, although only Δt_{FWM} is found to do so in experiment. This divergence is further discussed below.

The simulations can be rationalized by studying the corresponding dynamics of the density-matrix elements, as shown in Fig. 4e,f for both low (1 μW, 0.44 μJ cm^{-2}) and high (1 mW, 0.44 mJ cm^{-2}) pump powers. We

Fig. 5 | Simulated dependence of the delay time for maximal SFG and FWM on the lifetime of the excitonic states. a,b, Delay time for maximum SFG intensity as a function of the lifetime of state $|2\rangle$ (AX) (**a**) and state $|3\rangle$ (HX) (**b**) at a pump photon energy of 1.739 eV, one-photon resonant with the AX transition. **c,d**, Delay time for maximum FWM intensity as a function of the lifetime of state $|2\rangle$ (**c**) and state $|3\rangle$ (**d**) at a pump photon energy of 1.72 eV, two-photon resonant with the

HX transition. For all calculations, the probe photon energy is fixed at 1.476 eV. The lines are a guide to the eye. The delay time Δt_{SFG} is determined mainly by the lifetime of the one-photon resonant state $|2\rangle$, while the delay time Δt_{FWM} depends more strongly on the lifetime of the two-photon resonant state $|3\rangle$. The error bars mark the uncertainty in the peak position from fitting the numerical results.

propose that the largest SFG and FWM intensities are obtained when the centre of the probe pulse, that is, where the field strength is highest, coincides with the largest transient population of the excitonic state. Since both the AX state $|2\rangle$ and the HX state $|3\rangle$ have short but finite lifetimes, the state populations accumulate over the short timescale of the pump–probe pulse sequence. In the low-pump-power regime, maximum state occupancy then appears at positive delay times as seen in Fig. 4e. The delay times for maximal population of states $|2\rangle$ and $|3\rangle$ match well with Δt_{SFG} and Δt_{FWM}, respectively. As the pump power increases, however, the laser field becomes sufficiently strong, so that Rabi flopping in the state populations becomes relevant on the timescale of the interpulse delay. A detailed time evolution of the state population as a function of the pump power is shown in Supplementary Fig. 9. The signatures of the onset of this Rabi flopping have been studied in the context of SHG, when the two-photon resonance of the $|1\rangle \rightarrow |3\rangle$ HX transition is driven[20]. Rabi flopping is directly observed experimentally in the frequency domain, by examining the fingerprints of quantum interference in the SHG spectra as a function of the pulse length and amplitude—the number of transparency dips in the spectrum relates directly to the number of Rabi cycles undergone by the driven system in a single laser pulse[20]. Since the early depopulation of the excited states associated with Rabi flopping shifts maximum occupancy to earlier times (Fig. 4f), Δt_{SFG} and Δt_{FWM} decrease with increasing pump power (Fig. 4b,d).

Unlike in the experiments, however, the simulated Δt_{SFG} does turn negative. As we discussed in ref. [20], these density-matrix simulations do not include effects of many-body interactions such as enhanced Auger

recombination at high pump fluences and large exciton densities. We speculate that the efficient Auger-like exciton–exciton annihilation of band-edge excitons[28,36] in monolayer WSe_2 substantially raises the decay rate of state $|2\rangle$ at high exciton densities, and therefore prevents Δt_{SFG} from becoming negative. As shown in Fig. 5a,b, the simulated delay time Δt_{SFG} for maximum SFG intensity is very sensitive to the lifetime of state $|2\rangle$ and even approaches zero as this lifetime tends to zero. In stark contrast to this observation, Fig. 5c,d shows that Δt_{FWM} is mainly sensitive to the lifetime of state $|3\rangle$ but is quite insensitive to that of state $|2\rangle$.

The different dependencies of Δt_{SFG} and Δt_{FWM} on the lifetimes of the two states imply that SFG and FWM can be used to probe the dynamics of one-photon allowed and two-photon allowed excitonic states simultaneously but independently of each other. The largest experimentally observed delay time of $\Delta t_{SFG} = 120$ fs for bare WSe_2 corresponds to an AX lifetime of approximately 200 fs (Fig. 5a), which matches well with the population relaxation and radiative lifetime measured by transient intra- and interband spectroscopy[28] as well as optical two-dimensional Fourier-transform spectroscopy[29]. Although excitonic dynamics of one-photon allowed transitions are straightforward to probe using a variety of conventional optical means, the dynamics of two-photon allowed dark excitonic states have remained much more challenging to access, and our approach provides a simple solution to this problem.

In summary, we explored the influence of the delay between two laser pulses on second- and third-order optical wave-mixing processes in monolayer WSe_2. Substantial delays between the two pulses are found to be necessary to maximize the SFG and FWM signal intensities. Understanding these time delays poses challenges to the description

of spectroscopic observables in terms of the conventional picture of low-order perturbative nonlinear interactions[2]. The observations can, however, be rationalized in the framework of coherent population dynamics of the excitons under optical pumping as described within the density-matrix formalism, which computes the interaction of light and matter to arbitrary perturbative order. Further distinction between conventional parametric SFG and FWM and processes involving excitons will necessitate disentangling of the multitude of Liouville-space pathways embodied in the density-matrix time dynamics. The qualitative agreement between simulation and experiment suggests that the simplified ladder-type excitonic three-level system indeed captures the essential physical contributions to the delay effects observed in the optical wave mixing. Our work therefore demonstrates that nonlinear optical wave-mixing spectroscopy offers new opportunities for measuring the population dynamics of optically pumped excitonic states that are either one- or two-photon allowed, where the dynamics of the latter have proved challenging to access so far. The strong nonlinear interactions that enable the time delays to persist into the low-excitation regime promise to open up an as-yet unexplored regime of exciton-based quantum nonlinear optics in TMDC monolayers.

Online content

Any methods, additional references, Nature Research reporting summaries, source data, extended data, supplementary information, acknowledgements, peer review information; details of author contributions and competing interests; and statements of data and code availability are available at https://doi.org/10.1038/s41566-022-01080-1.

References

1. Shen, Y. R. *The Principles of Nonlinear Optics* (Wiley, 1984).
2. Boyd, R. W. *Nonlinear Optics* 3rd edn (Academic, 2008).
3. Keller, U. Recent developments in compact ultrafast lasers. *Nature* **424**, 831–838 (2003).
4. Garmire, E. Nonlinear optics in daily life. *Opt. Express* **21**, 30532–30544 (2013).
5. Mukamel, S. *Principles of Nonlinear Optical Spectroscopy* (Oxford University Press, 1999).
6. Cundiff, S. T. & Mukamel, S. Optical multidimensional coherent spectroscopy. *Phys. Today* **66**, 44–49 (2013).
7. Autere, A. et al. Nonlinear optics with 2D layered materials. *Adv. Mater.* **30**, 1705963 (2018).
8. Schneider, C. et al. Two-dimensional semiconductors in the regime of strong light–matter coupling. *Nat. Commun.* **9**, 2695 (2018).
9. Langer, F. et al. Lightwave valleytronics in a monolayer of tungsten diselenide. *Nature* **557**, 76–80 (2018).
10. Liu, H. et al. High-harmonic generation from an atomically thin semiconductor. *Nat. Phys.* **13**, 262–265 (2017).
11. You, J. W., Bongu, S. R., Bao, Q. & Panoiu, N. C. Nonlinear optical properties and applications of 2D materials: theoretical and experimental aspects. *Nanophotonics* **8**, 63–97 (2019).
12. Wang, G. et al. Colloquium: Excitons in atomically thin transition metal dichalcogenides. *Rev. Mod. Phys.* **90**, 021001 (2018).
13. Liu, G.-B. et al. Electronic structures and theoretical modelling of two-dimensional group-VIB transition metal dichalcogenides. *Chem. Soc. Rev.* **44**, 2643–2663 (2015).
14. Mak, K. F. & Shan, J. Photonics and optoelectronics of 2D semiconductor transition metal dichalcogenides. *Nat. Photonics* **10**, 216–226 (2016).
15. Lafeta, L. et al. Second- and third-order optical susceptibilities across excitons states in 2D monolayer transition metal dichalcogenides. *2D Mater.* **8**, 035010 (2021).
16. Hernandez-Rueda, J., Noordam, M. L., Komen, I. & Kuipers, L. Nonlinear optical response of a WS_2 monolayer at room temperature upon multicolor laser excitation. *ACS Photonics* **8**, 550–556 (2021).
17. Wang, G. et al. Giant enhancement of the optical second-harmonic emission of WSe_2 monolayers by laser excitation at exciton resonances. *Phys. Rev. Lett.* **114**, 097403 (2015).
18. Yao, K. et al. Continuous wave sum frequency generation and imaging of monolayer and heterobilayer two-dimensional semiconductors. *ACS Nano* **14**, 708–714 (2020).
19. Lin, K.-Q. et al. Narrow-band high-lying excitons with negative-mass electrons in monolayer WSe_2. *Nat. Commun.* **12**, 5500 (2021).
20. Lin, K.-Q., Bange, S. & Lupton, J. M. Quantum interference in second-harmonic generation from monolayer WSe_2. *Nat. Phys.* **15**, 242–246 (2019).
21. Fleischhauer, M., Imamoglu, A. & Marangos, J. P. Electromagnetically induced transparency: optics in coherent media. *Rev. Mod. Phys.* **77**, 633–673 (2005).
22. Phillips, M. C. et al. Electromagnetically induced transparency in semiconductors via biexciton coherence. *Phys. Rev. Lett.* **91**, 183602 (2003).
23. Kim, D.-S. et al. Unusually slow temporal evolution of femtosecond four-wave-mixing signals in intrinsic GaAs quantum wells: direct evidence for the dominance of interaction effects. *Phys. Rev. Lett.* **69**, 2725–2728 (1992).
24. Saiki, T., Kuwata-Gonokami, M., Matsusue, T. & Sakaki, H. Photon echo induced by two-exciton coherence in a GaAs quantum well. *Phys. Rev. B* **49**, 7817–7820 (1994).
25. Trovatello, C. et al. Optical parametric amplification by monolayer transition metal dichalcogenides. *Nat. Photonics* **15**, 6–10 (2021).
26. Dai, Y. et al. Electrical control of interband resonant nonlinear optics in monolayer MoS_2. *ACS Nano* **14**, 8442–8448 (2020).
27. Liu, S. et al. An all-dielectric metasurface as a broadband optical frequency mixer. *Nat. Commun.* **9**, 2507 (2018).
28. Poellmann, C. et al. Resonant internal quantum transitions and femtosecond radiative decay of excitons in monolayer WSe_2. *Nat. Mater.* **14**, 889–893 (2015).
29. Moody, G. et al. Intrinsic homogeneous linewidth and broadening mechanisms of excitons in monolayer transition metal dichalcogenides. *Nat. Commun.* **6**, 8315 (2015).
30. Cundiff, S. T. et al. Rabi flopping in semiconductors. *Phys. Rev. Lett.* **73**, 1178–1181 (1994).
31. Cadiz, F. et al. Excitonic linewidth approaching the homogeneous limit in MoS_2-based van der Waals heterostructures. *Phys. Rev. X* **7**, 021026 (2017).
32. Martin, E. W. et al. Encapsulation narrows and preserves the excitonic homogeneous linewidth of exfoliated monolayer $MoSe_2$. *Phys. Rev. Appl.* **14**, 021002 (2020).
33. Fang, H. H. et al. Control of the exciton radiative lifetime in van der Waals heterostructures. *Phys. Rev. Lett.* **123**, 067401 (2019).
34. Chang, D. E., Vuletić, V. & Lukin, M. D. Quantum nonlinear optics — photon by photon. *Nat. Photonics* **8**, 685–694 (2014).
35. Wild, D. S., Shahmoon, E., Yelin, S. F. & Lukin, M. D. Quantum nonlinear optics in atomically thin materials. *Phys. Rev. Lett.* **121**, 123606 (2018).
36. Sun, D. et al. Observation of rapid exciton–exciton annihilation in monolayer molybdenum disulfide. *Nano Lett.* **14**, 5625–5629 (2014).

Methods

Sample fabrication

The WSe_2 and WS_2 monolayers and thin layers of hBN were mechanically exfoliated from bulk single crystals (WSe_2 and WS_2, HQ Graphene; hBN, National Institute for Materials Science) using Nitto tape and transferred to a silicon substrate with a 90 nm silicon dioxide layer through stamping[37]. The hBN encapsulated monolayer WSe_2 sample was fabricated using a pick-up method[38]. The sample was cooled to 5 K using a microscope cryostat.

Nonlinear spectroscopy

A schematic of the experimental setup is depicted in Supplementary Fig. 1. A Ti:sapphire laser beam (Chameleon Ultra II, 80 MHz repetition rate, Coherent) was split using a 20:80 plate beamsplitter. The 20% reflected beam was used as the probe beam at the frequency ω_{probe}. The 80% transmitted beam was used to pump an optical parametric oscillator with intra-cavity frequency doubling (OPO-X fs, APE), which generates the pump beam at the frequency ω_{pump}. Both beams pass through custom-made prism-based pulse compressors to compensate their chirp, and a power-control unit was used to regulate the excitation power. The probe beam was directed through a delay stage and then combined with the pump beam through a 50:50 beamsplitter. The reflected beams were focused onto the sample surface inside a cryostat using a microscope objective (LUCPLFLN40X, 0.6NA, Olympus). The diameter of the laser spot was estimated to be 1.9 μm. The transmitted beams were focused into a BBO crystal that provides monitoring of the SFG signal measured using a photodiode, as detailed in Supplementary Note 1. The signal reflected from the sample passed through a 680 nm short-pass filter, was dispersed by a spectrometer (Acton SP2300, Princeton Instruments) and detected using a cooled CCD camera (PIXIS 100, Princeton Instruments). A 50:50 beamsplitter (BS3) was used to separate the excitation and emission beams.

Characterization of excitonic states

To characterize the AX of monolayer WSe_2, a 488 nm continuous-wave laser was focused onto the sample to excite the PL. To characterize the dark HX of monolayer WSe_2, an 80 fs pulsed Ti:sapphire laser (Mai Tai XF, 80 MHz repetition rate, Spectra-Physics) was focused onto the sample to drive the SHG. The PL signal after a 488 nm long-pass filter and the SHG signal after a 680 nm short-pass filter were measured using the same detection unit described for the nonlinear spectroscopy.

Density-matrix formalism simulation

The polarization in $P(t) \propto \sum_{ij} \mu_{ij} \rho_{ij}(t)$ is understood to be the source term for scattered radiation. Specific information about the SFG and FWM spectra was obtained by analysing $P(t)$ in the Fourier domain. We solved the time dynamics of the density matrix $\hat{\rho}$ in the framework of a Lindblad-type equation $\frac{d}{dt}\hat{\rho} = \frac{1}{i\hbar}[\hat{H},\hat{\rho}] - \frac{1}{2}\{\hat{\Gamma},\hat{\rho}\} + \hat{\Lambda}$. Here, the density matrix is defined in the conventional way as $\hat{\rho} = \sum_i p_i |i\rangle\langle i|$, with p_i the probability for the system to be in state $|i\rangle$. The Hamiltonian $\hat{H}$ is given by matrix elements $H_{ii} = E_i$ and $H_{ij} = -\varepsilon(t)\mu_{ij} (i \neq j)$, where E_i are the eigenstate energies, $\varepsilon(t)$ is the electric-field component of the incident light field and μ_{ij} are the transition dipole moments linked to the ρ_{ij} coherence. For simplicity, all vectorial properties of the field and the transition dipoles are neglected. The decay matrix $\hat{\Gamma}$ is diagonal with non-zero diagonal elements $\Gamma_{ii} = \Gamma_i (i > 1)$. The repopulation term $\hat{\Lambda}$ describes the repopulation of the ground state with a single non-zero matrix element $\Lambda_{11} = \sum_{i>1} \Gamma_i \rho_{ii}$. $\hbar$ is the reduced Planck constant.

Data availability

Any additional data are available from the corresponding authors upon reasonable request. Source data are provided with this paper.

Code availability

The Mathematica code used for the numerical simulations discussed in this paper is available from the corresponding authors upon reasonable request.

References

37. Castellanos-Gomez, A. et al. Deterministic transfer of two-dimensional materials by all-dry viscoelastic stamping. *2D Mater.* **1**, 011002 (2014).
38. Kim, K. et al. van der Waals heterostructures with high accuracy rotational alignment. *Nano Lett.* **16**, 1989–1995 (2016).

Author contributions

K.-Q.L. conceived and supervised the project. J.M.B., L.C., P.W., K.-Q.L. and S.B. carried out the experiments and simulations. S.B. wrote the simulation code. K.W. and T.T. provided the hBN crystals. All authors analysed the data, discussed the results and contributed to the writing of the manuscript.

Competing interests

The authors declare no competing interests.

Additional information

Supplementary information The online version contains supplementary material available at https://doi.org/10.1038/s41566-022-01080-1.

Correspondence and requests for materials should be addressed to Kai-Qiang Lin.

Peer review information *Nature Photonics* thanks Giulio Cerullo and Christoph Lienau for their contribution to the peer review of this work.

Reprints and permissions information is available at www.nature.com/reprints.